Experimental investigation of high-spin states in math xmlns="http://www.w3.org/1998/Math/MathML">mmultiscripts>mi>Zr/mi>mprescripts>/mprescripts>none>/none>mn>90/mn>/mmultiscripts>/math>

P. Dey et al.

Phys. Rev. C **105**, 044307 — Published 11 April 2022

DOI: 10.1103/PhysRevC.105.044307

Experimental investigation of high-spin states in ^{90}Zr

P. Dey[1],* D. Negi[1],† R. Palit[1],‡ P. C. Srivastava[2], Md S. R. Laskar[1], B. Das[1], F. S. Babra[1], S. Bhattacharya[3], Biswajit Das[1], K. Rojeeta Devi[4], R. Gala[1], U. Garg[5], S. S. Ghugre[6], E. Ideguchi[7], S. Kumar[4], A. Kundu[1], G. Mukherjee[8,9], S. Muralithar[10], S. Nag[11], S. Nandi[8,9], Neelam[4], M. Kumar Raja[12], R. Raut[6], R. Santra[1], A. Sharma[13], S. Sihotra[14], A. K. Singh[15], R. P. Singh[10], and T. Trivedi[3]

[1]*Deptartment of Nuclear and Atomic Physics, Tata Institute of Fundamental Research, Mumbai 400005, INDIA*
[2]*Department of Physics, Indian Institute of Technology Roorkee, Roorkee 247667, INDIA*
[3]*Department of Pure & Applied Physics, Guru Ghasidas Vishwavidyalaya, Bilaspur 495009, INDIA*
[4]*Department of Physics & Astrophysics, University of Delhi, Delhi 110007, INDIA*
[5]*Physics Department, University of Notre Dame, Notre Dame, Indiana 46556, USA*
[6]*UGC-DAE CSR Kolkata Centre, Kolkata 700098, INDIA*
[7]*Research Center for Nuclear Physics, Osaka University, Ibaraki, Osaka 567-0047, JAPAN*
[8]*Variable Energy Cyclotron Centre, 1/AF Bidhan Nagar, Kolkata 700064, INDIA*
[9]*Homi Bhabha National Institute, Anushaktinagar, Mumbai 400094, INDIA*
[10]*Inter University Accelerator Centre, Aruna Asaf Ali Marg, New Delhi 110067, INDIA*
[11]*Department of Physics, Indian Institute of Technology (Banaras Hindu University), Varanasi 221005, INDIA*
[12]*Department of Physics, GITAM Institute of Science, GITAM University, Visakhapatnam 530045, INDIA*
[13]*Department of Physics, Himachal Pradesh University, Summer Hill, Shimla 171005, INDIA*
[14]*Department of Physics, Panjab University, Chandigarh 160014, INDIA and*
[15]*Department of Physics, Indian Institute of Technology Kharagpur, Kharagpur 721302, INDIA*

High-spin states of ^{90}Zr have been investigated using the heavy-ion fusion-evaporation reaction ^{82}Se(^{13}C, $5n$) at a beam energy of 60 MeV. Excited levels of ^{90}Zr have been observed up to excitation energy $\sim$ 13 MeV and spin $\sim$ 20 $\hbar$ with the addition of thirty-two new gamma-ray transitions to the proposed level scheme. Structures of both the positive and negative parity states up to the highest observed spin have been interpreted with shell-model calculations using the GWBXG interaction and a ^{68}Ni core. Calculations suggest the role of neutron excitations across $N = 50$ shell gap for states above 7 MeV excitation energy. High-spin states in these bands are interpreted to be generated by the recoupling of stretched proton and neutron configurations.

I. INTRODUCTION

Nuclei in the vicinity of shell closures are of particular interest in nuclear structure studies as they provide a platform for scrutinizing the validity and details of shell model theories. It is now computationally feasible to extend the shell-model calculations to higher excitations, that incurs larger model space and increased number of valence nucleons, to be used for the purpose. High-spin states in the $A \sim 90$ mass region, with $Z \sim 40$ and $N \sim 50$, have been subjects of investigation in many studies, both experimentally and theoretically [1–31]. These states have multi-quasiparticle configurations, with the $g_{9/2}$ orbital playing a significant role towards the generation of high-spin states. The contribution of proton $g_{9/2}$ orbital comes into the picture either due to the (proton) particle occupancy of the orbital, that is for nuclei with $Z > 40$, or due to excitations of protons from the fp orbitals into the $g_{9/2}$ orbital across the $Z = 40$ subshell gap. These excitations dominate the lower energy part of the level scheme in these nuclei. Similarly, the role of neutron $g_{9/2}$ orbital towards the high-spin generation is seen either due to the already present holes in it, which is the case for nuclei with $N < 50$, or due to excitations across the $N = 50$ shell gap into the gd orbitals. Due to the larger energy of this gap, the contributions from these excitations underlying the high-spin states in $N = 50$ nuclei are observed at higher excitation energies. Such excitations of one or more neutrons from the $1g_{9/2}$ orbital into the $2d_{5/2}$ and $1g_{7/2}$ have been observed in the ^{86}Kr ($Z = 36$) [2], ^{87}Rb ($Z = 37$) [4], ^{88}Sr ($Z = 38$) [6], ^{89}Y ($Z = 39$) [11, 12], ^{91}Nb ($Z = 41$) [21], ^{92}Mo ($Z = 42$) [23], ^{93}Tc ($Z = 43$) [27], ^{94}Ru ($Z = 44$) [29] and ^{95}Rh ($Z = 45$) [31] isotones, it has yet to be confirmed in ^{90}Zr ($Z = 40$) [15]. The shell-model calculations have been successfully used to describe observed excited states based on either proton excitation across $Z = 40$ or neutron excitation across $N = 50$. It will be intriguing to invoke the two excitations simultaneously for ^{90}Zr, which is the focus of the present study.

Shell model calculations with the $\pi[1f_{5/2}, 2p, 1g_{9/2}]$, $\nu[2p_{1/2}, 1g_{9/2}]$ model space have been able to reproduce the experimental data reasonably well in ^{83}Br [32], ^{85}Rb [32], ^{87,88}Y [8, 10] up to a certain excitation energy ($\sim$ 5 MeV). The model space clearly seems to be inadequate for the description of high-spin states at higher excitation energies, where the role of $\nu[1g_{9/2}, 2d_{5/2}, 1g_{7/2}]$ orbitals due to excitation across the $N = 50$ shell gap increases. This is observed in the study of high-spin states of many

* piku.dey@tifr.res.in
† dinphysics@gmail.com
‡ palit@tifr.res.in

nuclei, *e.g.*, ^{88}Sr [6], ^{88}Y [10], ^{90,91,92}Zr [15, 18]. In the present study, shell model calculations have been performed involving these neutron orbitals to probe the role of these orbitals.

High-spin structures in this mass region have been observed to form $\Delta I = 1$ sequences of either parities with $M1$ transitions [6, 8, 15–17, 33, 34]. In ^{87}Y and ^{88}Sr, strong $B(M1)$ values have also been reported [6, 8]. The semiclassical model of shears mechanism has been used to describe a decreasing behaviour of $B(M1)$ strengths reported in ^{87}Zr [33]. Although, such $\Delta I = 1$, $M1$ sequences have been observed in ^{90}Zr by Warburton *et al.* [15], detailed information on the structure of these sequences could not be obtained owing to the inconclusive nature of their parity assignments. It is to be noted that the parity assignments of certain states, following the polarization measurements of different γ-ray transitions, are in disagreement. Recently, these sequences have been interpreted as examples of magnetic rotation [35], with the configuration assignments based on the parity assignments of Ref. [15]. The current work reports a detailed spectroscopic investigation of the ^{90}Zr nucleus. It has been directed at identifying new structural features in the high excitation regime as well as addressing the existing uncertainties in the assignments of properties for previously known transitions. The observed level scheme of the nucleus, upto the highest excitations, has been interpreted within the framework of shell-model calculations with large basis space.

II. EXPERIMENTAL DETAILS AND DATA ANALYSIS

Excited states of ^{90}Zr were populated using heavy-ion fusion-evaporation reactions ^{82}Se(^{13}C, $5n$)^{90}Zr with a 60 MeV ^{13}C beam provided by the TIFR-BARC Pelletron Linac Facility (PLF) at TIFR, Mumbai. The target used was 1 mg/cm^2 thick foil of ^{82}Se with a backing of ^{197}Au foil of thickness 4.3 mg/cm^2. The recoil velocity of the compound nucleus is $\sim 0.014c$. The γ-rays emitted in the reactions were detected with the Indian National Gamma Array (INGA) at TIFR, which is a Compton suppressed clover HPGe detector array with a provision of placing 24 detectors at various angles with respect to the beam direction [36]. During the experiment, a total of eleven clover detectors were placed at different angles, with two at 115°, and three each at 90°, 140° and 157°. The target to detector distance was 25 cm.

The electronic signal generated from the interaction of γ-rays with the detector were collected and processed with a digital data acquisition (DDAQ) system. The DDAQ system was housed in a compact PCI/PXI crate and consisted of six 12-bit 100 MHz Pixie-16 modules developed by XIA-LLC [37]. Each module has sixteen channels collecting signals from the individual crystals of clover detectors. A valid fast trigger of width 100 ns was generated for an event in a given channel of the Pixie-16 module in the absence of a veto pulse from the respective BGO Compton suppression shield within a specific time window. Each Compton suppressed clover detector generates a fast trigger of width 100 ns which is used for the gamma multiplicity in an event. Once the two- or higher-fold multiplicity is found, the master trigger was opened for 10 μs. This way the gamma-rays below the isomeric state could be found along with the prompt gamma-rays above the isomer. The data sorting program, Multi pARameter time-stamped based COincidence Search (MARCOS) [38], developed at TIFR, was used for sorting two- and higher-fold coincidence events into different E_γ-E_γ matrices and an E_γ-E_γ-E_γ cube, respectively. The RADWARE software package was used for data analysis [39, 40].

For the coincidence analysis, E_γ-E_γ matrices and E_γ-E_γ-E_γ cubes with different time windows (100 ns, 500 ns) around the prompt peak have been investigated. Efficiency and energy calibrations of the INGA are carried out using the ^{152}Eu and ^{133}Ba radioactive sources. The level scheme of the ^{90}Zr nucleus has been constructed from the coincidence relationships between the γ-rays, their intensities as well as their multipolarities and electromagnetic character, as determined through standard analysis techniques of γ-ray spectroscopy.

The spins of the levels are assigned through the measurements of the multipolarities of γ-ray transitions, which in turn are obtained from the angular distribution and directional correlation of oriented states (DCO) methods. The experimental angular distribution is given by the following expression [41],

$$W(\theta) = A_0[1 + a_2P_2(\cos\,\theta) + a_4P_4(\cos\,\theta)], \qquad (1)$$

where, A_0 is the normalization parameter, $P_n(\cos\,\theta)$ is the Legendre polynomial of order n and θ is the angle between the detector position and the beam axis. The angular distribution coefficients a_2 and a_4 were obtained from the χ^2-minimization of $W(\theta)$ to the observed yields at different angles.

The DCO method is incorporated by taking the ratios ($R_{\rm DCO}$) of intensities of coincident events detected at two different angles [42, 43]. In the present geometry of the INGA, the $R_{\rm DCO}$ is obtained using the expression,

$$R_{\rm DCO} = \frac{I(\gamma_1)\text{ at }157^\circ\text{ gated by }\gamma_2\text{ at }90^\circ}{I(\gamma_1)\text{ at }90^\circ\text{ gated by }\gamma_2\text{ at }157^\circ}, \qquad (2)$$

where, $I(\gamma_1)$ represents the intensity of γ_1 measured in coincidence with γ_2. The $R_{\rm DCO}$ values of stretched dipole and quadrupole transitions are $\sim$ 0.5 (1.0) and $\sim$ 1.0 (2.0), respectively, in a pure quadrupole (dipole) gate. Intermediate values of $R_{\rm DCO}$ between these values indicate mixed nature of the transitions.

The parity of an excited state is determined from the linear polarization measurement of the γ-ray transition emitted from that level. To identify the character, detectors at the angle 90° are used since at this angle the polarization measurements are most sensitive. This arrangement facilitates the use of clover detectors as Compton

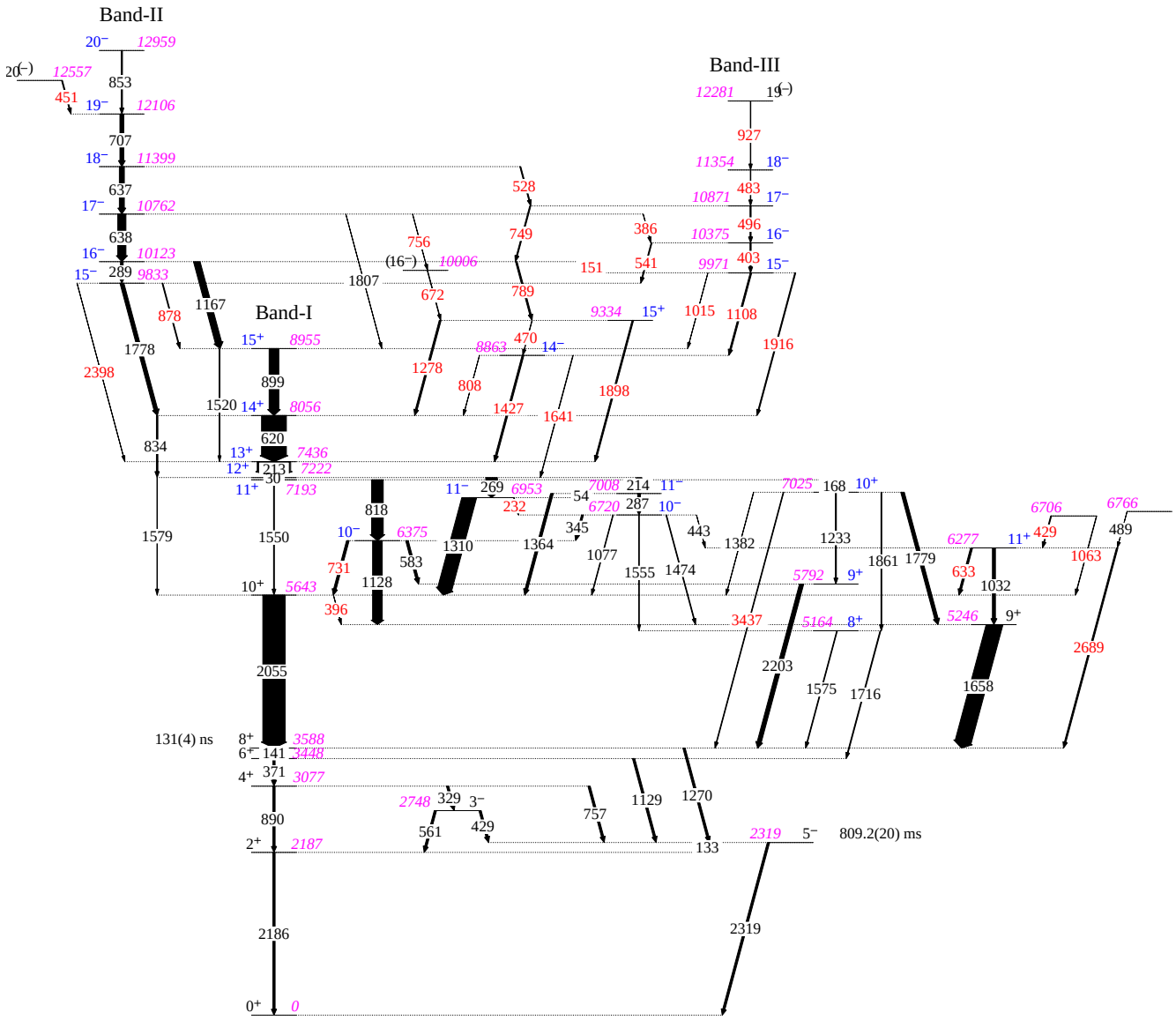

Figure 1. (Color online) Partial level scheme of ^{90}Zr developed in the present work. The energies of the excited states and γ-ray transitions are given in keV unit. The thickness of the arrows above the 3588 keV state are proportional to the γ-ray intensities mentioned in Table I. Newly observed gamma transitions are marked by red labels. The spin-parity of the levels marked by blue labels have been measured. The purple labels represent the level energies in keV unit. The experimentally observed values are given for γ-transition energy whereas the level energies are the output of the Gamma-to-Level (GTOL) least-squares fitting code developed at NNDC [46]. The transition energies and level energies shown in the level scheme have been rounded to the nearest whole numbers. The values of $t_{1/2}$ of 2319 and 3588 keV levels are adopted from Ref. [47].

polarimeters [44]. To extract the polarization asymmetry, integrated polarization directional correlation of oriented states (IPDCO) method was employed [45]. The electric or magnetic character of the γ-rays are determined from the asymmetry of the Compton scattered events to parallel and perpendicular directions. The polarization asymmetry of a transition, $\Delta_{\rm asym}$, is defined as,

$$\Delta_{\rm asym} = \frac{a(E_\gamma)N_\perp - N_\parallel}{a(E_\gamma)N_\perp + N_\parallel}, \qquad (3)$$

where $N_\perp(N_\parallel)$ is the intensity of γ-ray transitions scattered perpendicular (parallel) to the reaction plane and $a(E_\gamma)$ is a correction factor arising from any experimental asymmetry present. $a(E_\gamma)$ was determined from the ratio of parallel and perpendicular scattered events of unpolarized γ-rays from ^{133}Ba and ^{152}Eu radioactive sources. By fitting the experimentally observed $a(E_\gamma)$ values at different energies with a linear expression, $a(E_\gamma) = x + yE_\gamma$, we have obtained $x = +1.013(5)$ and $y = -2.1(8) \times 10^{-5}$ keV^{-1}. This result indicates a negligible dependence of $a(E_\gamma)$ on E_γ over the energy range considered for the

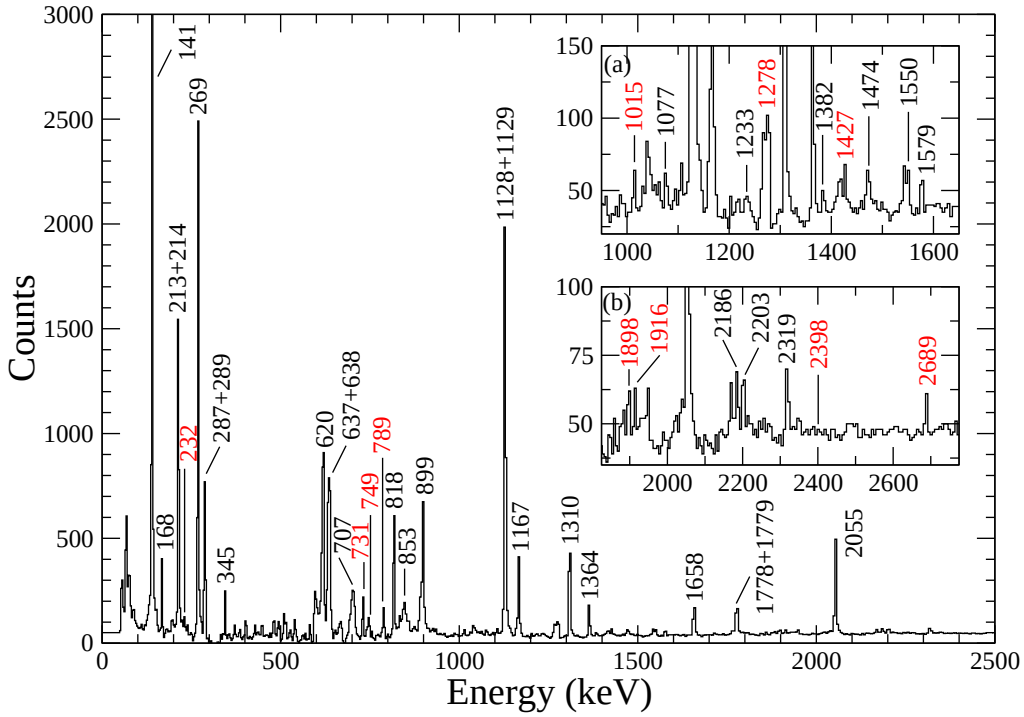

Figure 2. (Color online) Representative spectrum showing the sum of double-gated spectra with one gate on 213- and other on 620-, 1310-, 1658- and 2055-keV transitions. The newly observed transitions in ^{90}Zr are labelled in red color. The insets (a) and (b) depict the expanded energy ranges from 950 to 1650 keV and from 1825 to 2775 keV, respectively.

purpose.

For the determination of $\Delta_{\rm asym}$, two asymmetric matrices were constructed which contain events corresponding to parallel and perpendicular scattered γ-rays inside the 90° detectors in coincidence with γ-rays detected by any other detector of the array. A positive $\Delta_{\rm asym}$ value indicates the stretched $E1$, $E2$ or non-stretched $M1$ transition while a negative value implies stretched $M1$, $M2$ or non-stretched $E1$ transition.

III. RESULTS

The proposed level scheme of ^{90}Zr, resulting from the present analysis, is presented in Fig. 1. Properties of the levels and transitions determined from this work are reported in Table I. There is a 131(4) ns 8^+ isomer at 3588 keV excitation energy (see Fig. 1) which affects the measurements of relative intensities of the transitions across this isomeric state. The placement of transitions below this 8^+ level is made on the basis of relative yields determined from the total projection spectrum, and are found to be in agreement with earlier results [15]. The relative intensities of gamma transitions above the 8^+ level are determined from the total projection as well as gated spectra, and are normalized to that of the 2055-keV transition which feeds the 8^+ isomer. In the previous work on ^{90}Zr, Warburton *et al.* [15] reported levels up to the excitation energy $\sim$ 13 MeV and spin, $I = 20\ \hbar$, with tentative assignments for the levels above the 10^+ level at $E_x = 5643$ keV. In the present work, thirty-two new transitions have been added to the existing level scheme, and spin-parity of the levels have been determined. Two representative spectra, which are a sum of double-gated spectra, have been generated with gates on previously known γ-ray transitions, and are shown in Figs. 2 and 3. These gated spectra were generated from the E_γ-E_γ-E_γ cube with a coincidence time window of 500 ns. For the intensities, $R_{\rm DCO}$ and $\Delta_{\rm asym}$ measurements, the same coincidence time window has been used. The newly observed γ-ray transitions are marked in red in these figures and placed in the level scheme (Fig. 1). The 2319-keV transition shown in the inset (b) of Fig. 2 is emitted in the decay of 5^- isomeric state and it is essentially a constant background on the time scale of the coincidence windows. In the same gated spectrum (as Fig. 2) generated with the 100 ns time window, the 2319-keV peak is too weak and gets obscured by the background. This rules out the presence of additional 2319-keV transition in the level scheme.

Angular distribution measurements of some important γ-ray transitions of energies 818-, 1310-, and 2055-keV have been carried out. The results are in agreement with previously reported multipolarity assignments of these transitions [15]. The angular distribution measurements suggest, namely, $L = 1$ for the 818-, 1310-keV transitions and $L = 2$ for the 2055-keV transition. In Fig. 4, the angular distributions of relative yields,

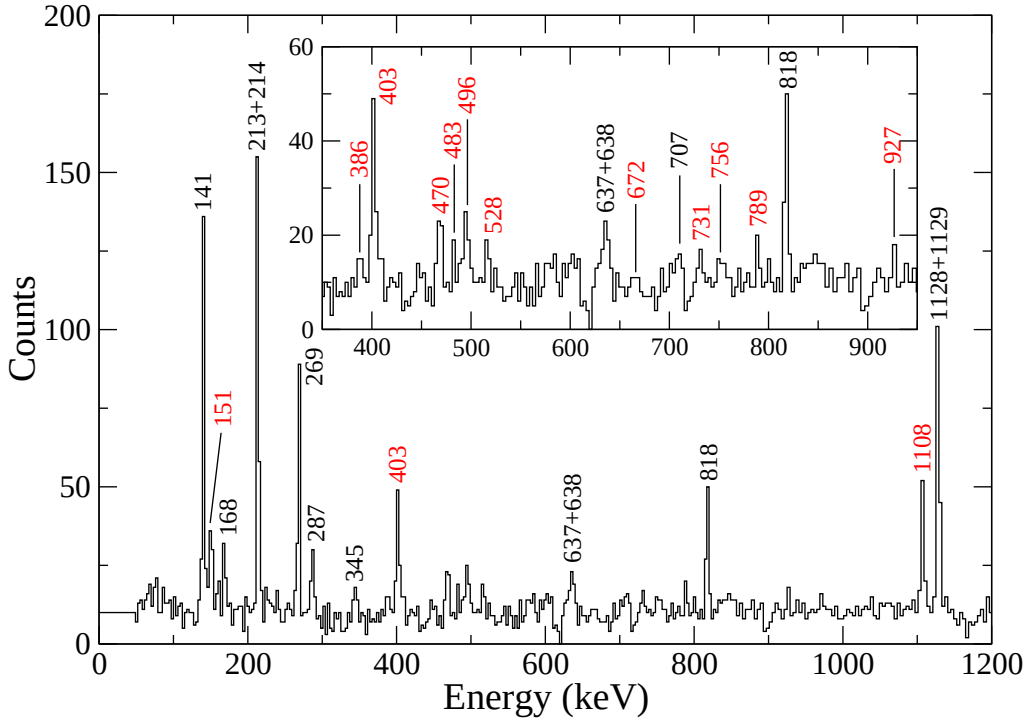

Figure 3. (Color online) Representative spectrum showing the sum of double-gated spectra with one gate on 1427- and other on 141-, 213-, 1310- and 2055-keV transitions. The newly observed transitions in ^{90}Zr are labelled in red color. The inset shows the expanded energy range from 300 to 1000 keV for a better view of the weaker transitions.

$W(\theta)/A_0$, for the 2055-, 1310- and 818-keV gamma transitions are presented. In addition, the positive values of $\Delta_{\rm asym}$ suggest their electric character. These transitions have primarily been used as reference transitions for the $R_{\rm DCO}$ of other transitions in the level scheme. The $R_{\rm DCO}$ and $\Delta_{\rm asym}$ measurements for the 213- and 269-keV transitions suggest them as stretched $M1$ and $E1$ transitions, respectively. Additionally, a small mixing ratio ($\delta = +0.034^{+0.037}_{-0.042}$) of the 213-keV transition indicates very little $E2$ mixing and thus, it can be regarded as a pure dipole transition. These two transitions are also used as reference transitions for the DCO ratio measurements.

A new sequence of levels, referred to as Band-III, has been observed. For clarity in discussion, the whole level scheme is divided into four groups, which are labeled as Band-I, Band-II, Band-III, and the other states in Fig. 1.

A. Band-I

The levels at 7193, 7222, 7436, 8056, and 8955 keV are included in this band. These levels were observed in the earlier work as well [15], but their spin assignments were tentative. In this study, we have determined the spin-parity assignment of these levels. The spin-parity assignment of the 7222 keV level is confirmed as 12^+, following the determination of the 1310- and 269-keV transitions as $E1$. Above the 12^+ state, the transitions of the band are determined as $M1$. This agrees with the previously reported positive-parity assignment up to the 14^+ level at 8056 keV excitation energy. The 899-keV transition is assigned as $M1$ type based on the polarization measurement which was previously reported as $E1$ character [15]. The final value of $\Delta_{\rm asym} = -0.041(5)$ for this transition is obtained by taking weighted average of $\Delta_{\rm asym}$ determined individually from the coincidence spectra with gates on the 213-, 269-, 818-, 1167-, 1310- and 2055-keV transitions. It is important to note that the 898-, 899-, and 901-keV transitions from ^{88}Sr [6], ^{90}Y [13], and ^{91}Zr [18], respectively, can be the contaminants for the polarization measurements for the fusion-evaporation reactions used for the study of ^{90}Zr in the present as well as previous measurement [15]. Gating on transitions of ^{90}Zr ensured the elimination of possible contaminants, especially the one coming from ^{91}Zr. In addition, two weak crossover $E2$ transitions of 834-keV ($14^+ \rightarrow 12^+$) and 1520-keV ($15^+ \rightarrow 13^+$) are confirmed which were reported tentatively in previous work [15].

B. Band-II

A sequence of levels inter-connected by $M1$ transitions has been observed. This sequence has been observed in the earlier work too, where its parity was tentatively assigned as positive [15]. However, the new identification

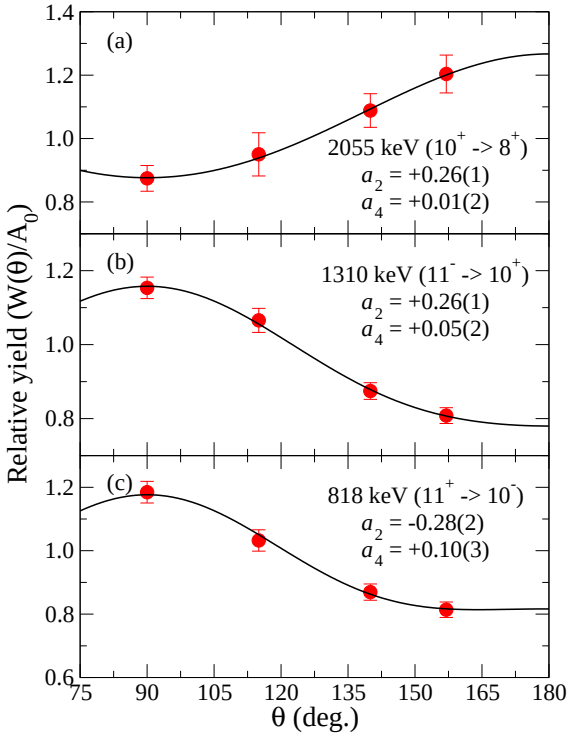

Figure 4. (Color online) Angular distribution of – (a) $L = 2$, 2055-keV ($10^+ \rightarrow 8^+$), (b) $L = 1$, 1310-keV ($11^- \rightarrow 10^+$) and (c) $L = 1$, 818-keV ($11^+ \rightarrow 10^-$) γ-transitions in ^{90}Zr. The experimental data is represented by filled red circles and the fitted curve by black solid line. The errors in relative yield have been multiplied by a factor of 2 for a better view.

of the 899-keV transition of Band-I as $M1$ transition in conjunction with the confirmation of the 1167-keV transition, connecting the 10123 keV level of the Band-II to the 8955 keV 15^+ level of Band-I, as $E1$ transition, suggests the parity of the band to be negative. Further confirmation comes from the measurements on the 1778-keV transition, which is identified as $E1$ transition. Although this identification is consistent with the polarization measurement done by Warburton *et al.*, which has a positive value (see Table III of Ref. [15]), the transition was ascribed as $M1$. Owing to the contaminations of 1778-keV transition reported in Ref. [15], the multipolarity assignment for this transition was tentative in the previous work [15]. In the present study, the possibility of placing gates on specific transitions towards the measurement of 1778-keV transition resolves this issue. In addition, we confirm the $M1$ assignment for the 638-, 637-, 707-, and 853-keV gamma transitions of the band (see Table I). Within the sensitivity limit of the present experiment, no cross-over $E2$ transitions have been observed in this band. Levels of this band has also been observed to decay to the levels of Band-I by multiple pathways. This includes the pathway via the newly-identified levels at 8863, 9334, and 10006 keV. In addition, two new transitions *viz.* 878- and 2398-keV are observed to decay from the 9833 keV, 15^- level of the band to that of Band-I.

C. Band-III

A new level at $E_x = 8863$ keV has been observed which decays to the 7436 keV level through a 1427-keV transition. The results of $R_{\rm DCO}$ and $\Delta_{\rm asym}$ measurements suggest an $E1$ multipolarity, and thereby suggest the spin and parity of the level at 8863 keV as 14^-. This level is connected, via the 1108-keV transition of $M1 + E2$ type, to a new sequence of levels observed for the first time in this nucleus. Levels of this band have been determined as negative parity levels connected by $M1$ transitions. However, the parity of the topmost level, decaying by 927-keV transition, is kept tentative as the $\Delta_{\rm asym}$ could not be determined for this transition due to limited statistics. Some of these levels are also observed to be connected to the levels of Band-I and Band-II. Additionally, the polarization measurement of the 1916-keV transition, which suggests its $E1$ multipolarity, connecting to the 8056 keV level of Band-I, provides further support to the negative parity assignment of the levels of this band.

D. Other states

In this group, levels at energies 5164, 5246, 5792, 6277, 6375, 6720, 6953, 7008 and 7025 keV are included. Most of the spin-parity assignments of the levels in this group were tentative before this work. These assignments are now confirmed through the DCO ratio and polarization measurements. Several new transitions of energies 232-, 396-, 633-, 731-, 2689-, and 3437-keV are added to the level scheme (see Fig. 1). However, no transition between 7222 keV, 12^+ level of Band-I and 6277 keV, 11^+ level has been observed in this work. In addition, 6766 keV level has been observed and a new level at 6706 keV excitation energy have been added. Due to the lack of statistics for the decay transitions from these levels, their the spin-parity assignments were not possible.

Table I: Table for level energy (E_i) and spin-parity of the states, and γ-ray energy (E_γ), intensity (I_γ), $R_{\rm DCO}$, $\Delta_{\rm asym}$ and multipolarity of the transitions obtained from this work. The γ-ray and level energies are given up to the first decimal values in the table. These values are rounded to the nearest whole numbers in the figures and text.

E_γ [a] (keV)	Intensity (I_γ)[b]	Level energy (E_i) (keV)	DCO ratio ($R_{\rm DCO}$) $L = 1$ gate[c]	DCO ratio ($R_{\rm DCO}$) $L = 2$ gate[d]	Polarization asym. ($\Delta_{\rm asym}$)	Multipolarity	$I_i^\pi \longrightarrow I_f^\pi$
Below 3588							

E_γ [a] (keV)	Intensity (I_γ)[b]	Level energy (E_i) (keV)	DCO ratio ($R_{\rm DCO}$) $L=1$ gate[c]	DCO ratio ($R_{\rm DCO}$) $L=2$ gate[d]	Polarization asym. ($\Delta_{\rm asym}$)	Multipolarity	$I_i^\pi \longrightarrow I_f^\pi$
keV level							
132.7		2319.1					$5^- \longrightarrow 2^+$
140.7		3588.4					$8^+ \longrightarrow 6^+$
328.5		3076.6					$4^+ \longrightarrow 3^-$
370.8		3447.9					$6^+ \longrightarrow 4^+$
429.3		2748.1					$3^- \longrightarrow 5^-$
561.1		2748.1					$3^- \longrightarrow 2^+$
757.4		3076.6					$4^+ \longrightarrow 5^-$
890.1		3076.6					$4^+ \longrightarrow 2^+$
1128.8		3447.9					$6^+ \longrightarrow 5^-$
1270.0		3588.4					$8^+ \longrightarrow 5^-$
2186.4		2186.7					$2^+ \longrightarrow 0^+$
2319.1		2319.1					$5^- \longrightarrow 0^+$
Above 3588 keV level							
29.6[e]		7222.2					$12^+ \longrightarrow 11^+$
54.4	1.81(19)	7007.6					$11^- \longrightarrow 11^-$
151.3	2.31(15)	10122.6	0.92(15)[f]			$M1$[g]	$16^- \longrightarrow 15^-$
168.2	20(2)	7192.8	1.06(11)[h]	0.52(9)		$M1$[g]	$11^+ \longrightarrow 10^+$
213.3	150(12)	7435.6	1.08(8)[i]	0.53(4)[j]	−0.049(7)	$M1$	$13^+ \longrightarrow 12^+$
214.4[k]	26(2)	7222.2	1.03(10)[f]			$E1$[g]	$12^+ \longrightarrow 11^-$
232.2	2.82(15)	6952.8	0.88(9)[l]		−0.019(96)	$M1$	$11^- \longrightarrow 10^-$
269.4	52(3)	7222.2	1.12(6)[f]	0.52(3)	+0.104(7)	$E1$	$12^+ \longrightarrow 11^-$
287.0	12.27(94)	7007.6	0.96(8)[h]	0.55(8)	−0.016(38)	$M1$	$11^- \longrightarrow 10^-$
289.2	12.00(52)	10122.6	0.89(6)[f]	0.36(4)	−0.070(42)	$M1$	$16^- \longrightarrow 15^-$
344.8	8.54(43)	6720.0	2.07(17)[h]		+0.096(32)	$(E2)$	$10^- \longrightarrow 10^-$
386.4	1.19(8)	10761.7					$17^- \longrightarrow 16^-$
396.4	1.07(5)	5643.2					$10^+ \longrightarrow 9^+$
403.2	5.05(33)	10374.7	0.87(9)[i]	0.41(5)	−0.073(32)	$M1$	$16^- \longrightarrow 15^-$
429.2[m]	3.83(10)	6706.3	0.78(8)[h]		−0.043(65)	$(M1+E2)$	$\longrightarrow 11^+$
443.1	$\sim 0.5(1)$	6720.0					$10^- \longrightarrow 11^+$
450.8	4.16(44)	12556.9	1.21(12)[h]		−0.017(75)	$M1+E2$	$20^{(-)} \longrightarrow 19^-$
470.3	1.60(8)	9333.5					$15^+ \longrightarrow 14^-$
483.1	2.17(19)	11354.2	0.92(8)[h]	0.61(5)	−0.048(53)	$M1$	$18^- \longrightarrow 17^-$
489.3	< 0.5	6766.4					$\longrightarrow 11^+$
496.3	4.78(42)	10871.1	0.82(7)[h]		−0.032(24)	$M1$	$17^- \longrightarrow 16^-$
528.4	4.32(32)	11399.3	0.86(9)[h]		−0.086(60)	$M1$	$18^- \longrightarrow 17^-$
541.1	4.03(24)	10374.7	1.11(9)[h]		−0.026(30)	$M1$	$16^- \longrightarrow 15^-$
583.3	11.41(69)	6374.8	0.83(3)[i]		+0.035(24)	$E1$	$10^- \longrightarrow 9^+$
619.7	111(3)	8055.6	0.79(2)[f]	0.35(1)	−0.049(3)	$M1+E2$	$14^+ \longrightarrow 13^+$
633.2	8.99(41)	6277.1					$11^+ \longrightarrow 10^+$
637.4[n]	22(2)	11399.3	0.78(3)[f]	0.44(2)	−0.042(5)	$M1$	$18^- \longrightarrow 17^-$
638.3[n]	36.51(88)	10761.7	0.78(3)[f]	0.44(2)	−0.042(5)	$M1$	$17^- \longrightarrow 16^-$
671.8	2.01(9)	10005.6	0.72(7)[l]		+0.024(18)	$(E1)$	$(16^-) \longrightarrow 15^+$
706.8	17(2)	12106.1	1.08(8)[h]		−0.063(11)	$M1$	$19^- \longrightarrow 18^-$
731.1	11.26(31)	6374.8	2.09(12)[i]	0.89(4)	−0.076(21)	$E1$	$10^- \longrightarrow 10^+$
748.7	4.88(46)	10871.1	0.84(7)[h]		−0.128(24)	$M1$	$17^- \longrightarrow 16^-$
755.9	1.15(6)	10761.7					$17^- \longrightarrow (16^-)$
789.3	6.99(22)	10122.6	0.86(9)[f]		+0.033(30)	$E1$	$16^- \longrightarrow 15^+$
808.2	< 0.5	8863.3					$14^- \longrightarrow 14^+$
818.0	52(2)	7192.8	0.87(6)[h]	0.55(4)	+0.045(6)	$E1$	$11^+ \longrightarrow 10^-$
833.7	6.45(51)	8055.6	1.51(12)[l]		+0.045(42)	$(E2)$[o]	$14^+ \longrightarrow 12^+$
853.1	5.41(55)	12959.2	1.09(9)[h]		−0.055(18)	$M1$	$20^- \longrightarrow 19^-$
878.1	3.62(11)	9833.4	1.47(20)[h]		−0.102(91)	$E1$	$15^- \longrightarrow 15^+$
899.1	43(2)	8955.1	0.90(2)[i]	0.46(2)	−0.041(5)	$M1$	$15^+ \longrightarrow 14^+$
926.6	2.00(18)	12280.8	1.43(18)[h]			$(M1+E2)$	$19^{(-)} \longrightarrow 18^-$
1014.7	$\sim 0.5(1)$	9971.1					$15^- \longrightarrow 15^+$

E_γ [a] (keV)	Intensity (I_γ)[b]	Level energy (E_i) (keV)	DCO ratio ($R_{\rm DCO}$) $L=1$ gate[c]	$L=2$ gate[d]	Polarization asym. ($\Delta_{\rm asym}$)	Multipolarity	$I_i^\pi \longrightarrow I_f^\pi$
1031.6	13.35(71)	6277.1	1.84(26)[h]		+0.094(35)	$E2$	$11^+ \longrightarrow 9^+$
1063.1	1.64(8)	6706.3					$\longrightarrow 10^+$
1076.8	2.58(11)	6720.0	1.92(22)[h]	1.14(13)	−0.080(68)	$E1$	$10^- \longrightarrow 10^+$
1108.0	6.62(41)	9971.1	0.66(7)[h]	0.43(9)	+0.059(57)	$M1+E2$	$15^- \longrightarrow 14^-$
1128.4[p]	43(3)	6374.8	1.06(2)[i]		+0.021(3)	$E1$	$10^- \longrightarrow 9^+$
1167.3	28.69(71)	10122.6	0.92(4)[f]	0.39(2)	+0.023(8)	$E1$	$16^- \rightarrow 15^+$
1233.4	4.36(25)	7025.1	0.88(10)[h]		−0.032(44)	$M1$	$10^+ \longrightarrow 9^+$
1277.5	8.10(35)	9333.5	0.78(7)[f]		−0.069(51)	$M1+E2$	$15^+ \longrightarrow 14^+$
1309.7	64(2)	6952.8		0.46(1)	+0.017(5)	$E1$	$11^- \longrightarrow 10^+$
1364.4	11.94(34)	7007.6	0.83(6)[h]	0.45(2)	+0.024(15)	$E1$	$11^- \longrightarrow 10^+$
1381.6	1.15(6)	7025.1	1.86(40)[h]	0.87(23)		$(E2)$[g]	$10^+ \longrightarrow 10^+$
1427.4	7.82(20)	8863.3	0.82(6)[h]	0.44(6)	+0.032(29)	$E1$	$14^- \longrightarrow 13^+$
1473.6	3.04(15)	6720.0	1.06(10)[h]		+0.032(45)	$E1$	$10^- \longrightarrow 9^+$
1519.9	$\sim 0.5(1)$	8955.1					$15^+ \longrightarrow 13^+$
1550.3	3.58(14)	7192.8	0.51(6)[h]		−0.005(78)	$M1+E2$	$11^+ \longrightarrow 10^+$
1554.5	< 0.5	6720.0					$10^- \longrightarrow 8^+$
1574.9	3.08(10)	5164.3	1.36(19)[h]				$8^+ \longrightarrow 8^+$
1579.0	1.90(8)	7222.2	1.90(34)[h]	1.03(21)	+0.095(135)	$E2$	$12^+ \longrightarrow 10^+$
1641.3	1.79(9)	8863.3					$14^- \longrightarrow 12^+$
1658.1	73(2)	5246.4	1.43(3)[i]		−0.051(7)	$M1+E2$	$9^+ \longrightarrow 8^+$
1716.3	3.60(17)	5164.3	1.79(22)[h]		+0.073(93)	$E2$	$8^+ \longrightarrow 6^+$
1777.7	17.10(86)	9833.4	0.73(5)[f]	0.39(3)	+0.025(28)[q]	$E1$	$15^- \longrightarrow 14^+$
1778.9[r]	15(2)	7025.1					$10^+ \longrightarrow 9^+$
1807.0	< 0.5	10761.7					$17^- \longrightarrow 15^+$
1861.1	3.32(19)	7025.1	2.23(25)[h]		+0.070(92)	$E2$	$10^+ \longrightarrow 8^+$
1898.1	6.39(20)	9333.5	1.59(20)[l]		+0.126(86)	$(E2)$[o]	$15^+ \longrightarrow 13^+$
1915.9	4.30(15)	9971.1	0.74(14)[h]		+0.036(58)	$E1$	$15^- \longrightarrow 14^+$
2054.7	100(2)	5643.2	2.01(6)[f]		+0.017(7)	$E2$	$10^+ \longrightarrow 8^+$
2202.8	18.53(54)	5791.5	0.99(5)[i]		−0.053(16)	$M1$	$9^+ \longrightarrow 8^+$
2398.0	< 0.5	9833.4					$15^- \longrightarrow 13^+$
2688.7	6.60(22)	6277.1					$11^+ \longrightarrow 8^+$
3437.3	2.85(20)	7025.1	1.60(19)[h]			$(E2)$[o]	$10^+ \longrightarrow 8^+$

[a] The uncertainties of γ-ray energy centroids of strong ($I_\gamma \geq 15$) and weak ($I_\gamma < 15$) transitions are around 0.3 and 0.6 keV, respectively.

[b] Internal conversion corrected intensities of γ-ray transitions above the 8^+ state are normalized to the 2054.7-keV transition.

[c] $R_{\rm DCO}$ values are obtained using stretched dipole transitions as gate.

[d] $R_{\rm DCO}$ values are obtained using the 2054.7-keV gate (quadrupole transition).

[e] Not observed in this work, energy taken from Ref. [15].

[f] $R_{\rm DCO}$ values are obtained using the 1309.7-keV gate.

[g] Multipolarity assignment is based on the $R_{\rm DCO}$ measurements and the spin-parity of the initial and final levels. These spin-parity are determined from the measurements on other strong transitions.

[h] $R_{\rm DCO}$ values are obtained using the 213.3-keV gate. The mixing ratio of the 213.3-keV $M1$ transition is, $\delta = +0.034^{+0.037}_{-0.042}$.

[i] $R_{\rm DCO}$ values are obtained using the 818.0-keV gate.

[j] Contains contributions from the 214.4-keV transition ($E_x = 7222.2$ keV, $12^+ \rightarrow 11^-$).

[k] For $\Delta_{\rm asym}$ measurements, no strong transition as a gate is possible to eliminate contributions from the 213.3-keV transition ($E_x = 7435.6$ keV, $13^+ \rightarrow 12^+$). The $R_{\rm DCO}$ is measured for unresolved (213.3 + 214.4)-keV transition.

[l] $R_{\rm DCO}$ values are obtained using the 269.4-keV gate.

[m] The $R_{\rm DCO}$ and $\Delta_{\rm asym}$ have contributions from another 429.3-keV transition ($E_x = 2748.1$ keV, $3^- \rightarrow 5^-$).

[n] The $R_{\rm DCO}$ and $\Delta_{\rm asym}$ are obtained for unresolved (637.4+638.3)-keV transition. The multipolarity assignments have been made on the basis of these values.

[o] The spin-parity of the initial and final levels of the marked transitions are determined from other strong transitions. $R_{\rm DCO}$ value is notably smaller compared to the expected value for stretched $E2$ transition indicating possible mixing of higher multipolarity, which needs further investigation. Multipolarity assignment has therefore been made tentative.

[p] The $R_{\rm DCO}$ and $\Delta_{\rm asym}$ have contributions from another 1128.8-keV transition ($E_x = 3447.9$ keV, $6^+ \rightarrow 5^-$).

[q] Transitions parallel to the 1778.9-keV ($E_x = 7025.1$ keV, $10^+ \rightarrow 9^+$) transition are used as gate.

[r] For $R_{\rm DCO}$ and $\Delta_{\rm asym}$ measurements, no strong transition as a gate is possible to eliminate contributions from the 1777.7-keV transition ($E_x = 9833.4$ keV, $15^- \rightarrow 14^+$).

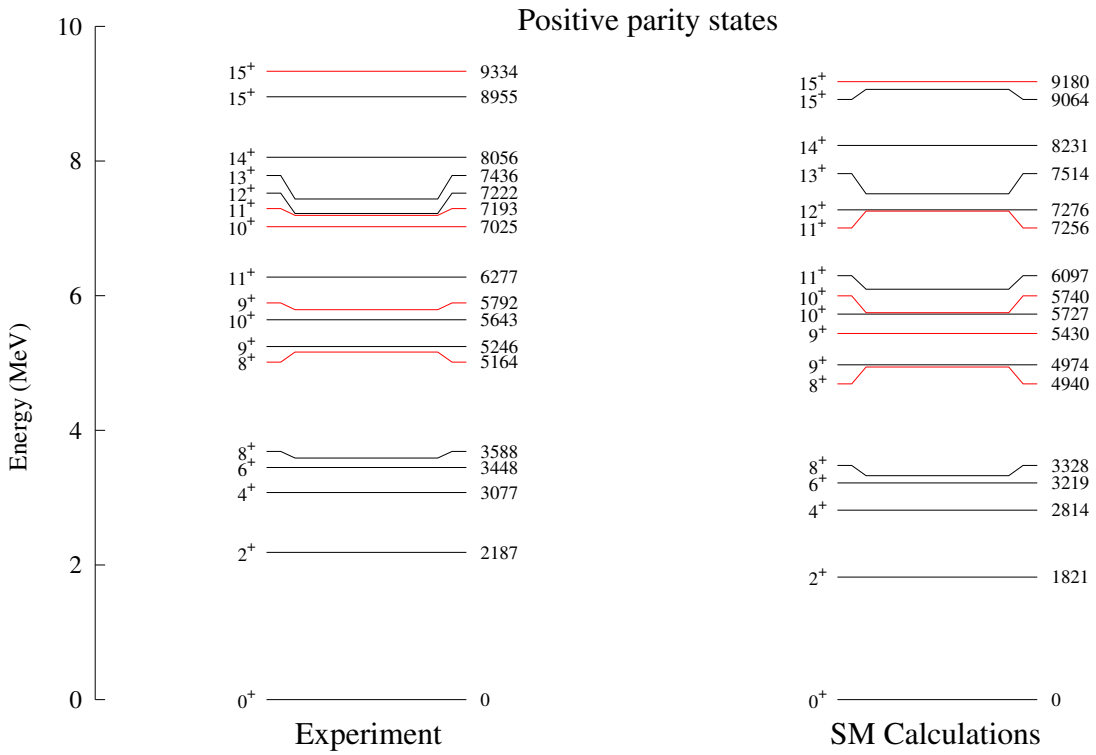

Figure 5. (Color online) A comparison of the experimental excitation energies of the positive parity states (left) of ^{90}Zr with those from shell-model calculation using the GWBXG effective interaction (right). For a given spin whenever more than one state is present, they have been marked with red (second excited state).

IV. THEORETICAL CALCULATIONS AND DISCUSSION

^{90}Zr has $Z = 40$ and $N = 50$, making it a semimagic nucleus. As a consequence, the structure of its low lying states displays characteristic features of a spherical nucleus, *i.e.*, they are described quite successfully within the scope of shell-model with a spherical mean field. Even at the high-spin and excitation energies, observed so far, the absence of strong $E2$ transitions suggests no appreciable collectivity.

Early shell-model calculations for ^{90}Zr were performed with a smaller model space, where protons were restricted to the $1f_{5/2}, 2p_{3/2}, 2p_{1/2}, 1g_{9/2}$ orbitals, while the neutron $2p_{1/2}, 1g_{9/2}$ orbitals were completely filled [1]. In later study, it is shown to be necessary to include the neutron orbitals above the $N = 50$ shell gap in the model space for the description of states with spin $I > 12\ \hbar$, although good agreement with experimental data is reported for states below $I = 12\ \hbar$ [15, 48]. High-spin states in many nuclei in this mass region *viz.* ^{86}Kr [2], ^{88}Kr [3], ^{87}Rb [4], ^{89}Rb [3], ^{88}Sr [6], ^{89,90}Sr [7], ^{89}Y [11, 12], ^{90}Y [13], ^{91}Y [14], ^{91,92}Zr [18], ^{91}Nb [21], ^{92}Mo [23], ^{93}Mo [24], ^{94}Mo [25], ^{93}Tc [27], ^{94}Tc [28], ^{94}Ru [29], ^{95}Ru [30] and ^{95}Rh [31] have been studied using the extended model space with the inclusion of neutron orbitals above $N = 50$ shell gap.

A. Shell-model calculations

To interpret the experimental data, we have performed shell-model calculations using the GWBXG effective interaction with ^{68}Ni core. The GWBXG interaction has $1f_{5/2}, 2p_{3/2}, 2p_{1/2}, 1g_{9/2}$ proton orbitals and $2p_{1/2}$, $1g_{9/2}$, $1g_{7/2}$, $2d_{5/2}$, $2d_{3/2}$ and $3s_{1/2}$ neutron orbitals. The single-particle energies (in MeV) used in this interaction are $1f_{5/2} = -5.322$, $2p_{3/2} = -6.144$, $2p_{1/2} = -3.941$, $1g_{9/2} = -1.250$ for the proton orbitals, and $2p_{1/2} = -0.696$, $1g_{9/2} = -2.597$, $1g_{7/2} = +5.159$, $2d_{5/2} = +1.830$, $2d_{3/2} = +4.261$, $3s_{1/2} = +1.741$ for the neutron orbitals. In our calculations for the neutrons we have completely filled $2p_{1/2}$, while we have not allowed any neutrons to occupy in $1g_{7/2}$ and $2d_{3/2}$ orbitals. Further, since the dimension is very large, we have allowed a maximum of one neutron each in the $2d_{5/2}$ and $3s_{1/2}$ orbitals. Calculations are performed with the shell-model code KSHELL [49]. The GWBXG effective interaction is constructed with different interactions. The original 974 two-body matrix elements (TBMEs) are obtained from bare G-matrix of the H7B potential [50]. The bare G-matrix is not reasonable because of the space truncation

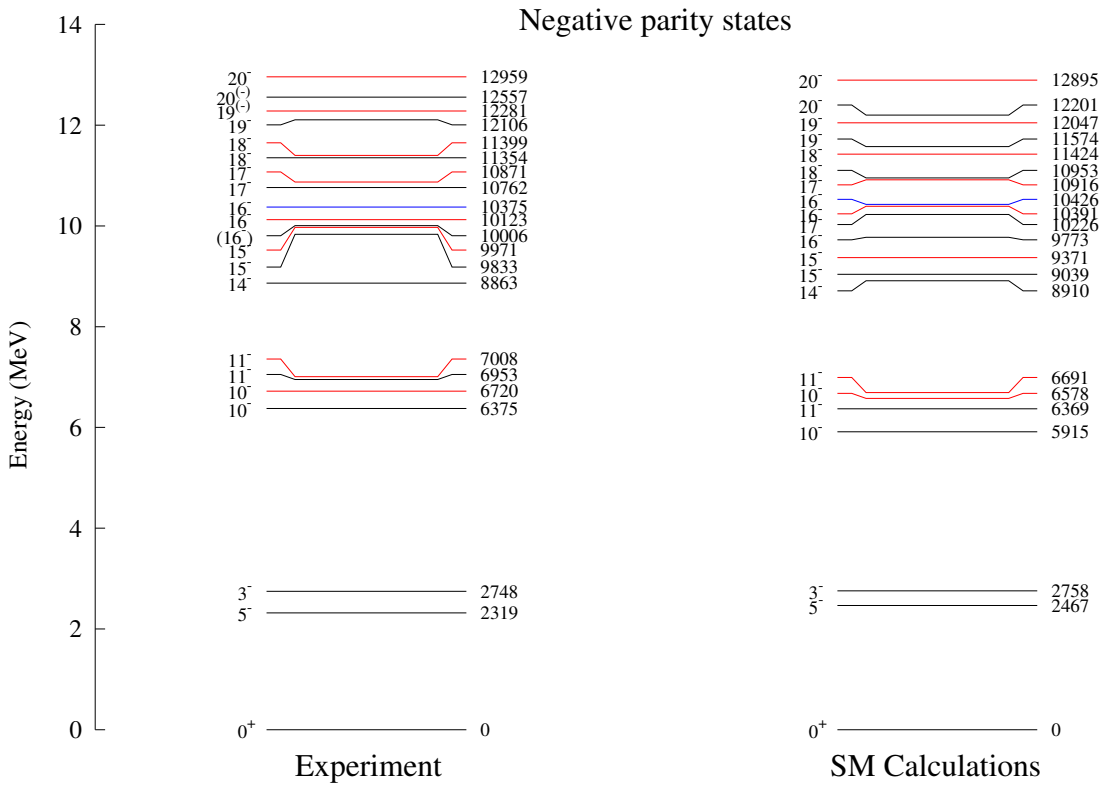

Figure 6. (Color online) A comparison of the experimental excitation energies of the negative parity states (left) of ^{90}Zr with those from shell-model calculation using the GWBXG effective interaction (right). For a given spin whenever more than one state is present, they have been marked with red (second excited state) and blue (third excited state).

and the interaction should be renormalized by taking into account the core-polarization effects. Here, the present G-matrix effective interaction is further tuned by modifying matrix elements with fitted interactions by following way. The 65 TBMEs for proton orbitals are replaced with the effective values reported in Ref. [51]. The TBMEs connecting the $\pi(2p_{1/2}, 1g_{9/2})$ and the $\nu(2d_{5/2}, 3s_{1/2})$ orbitals are replaced by those from the work of Gloeckner [52]. The TBMEs between the $\pi(2p_{1/2}, 1g_{9/2})$ and the $\nu(2p_{1/2}, 1g_{9/2})$ orbitals are replaced with the values determined by Serduke *et al.* [53]. Earlier, shell-model results for high-spin states for ^{91}Y and ^{95}Nb using this interaction have been reported in Ref. [14]. Also, the positive-parity yrast states of the neutron-rich ^{89}Rb, ^{92}Y, and ^{93}Y nuclei using the same interaction have been reported in Ref. [54].

The calculated results for spin up to $I = 15\ \hbar$ and excitation energy of around 9 MeV for positive parity states, while $I = 20\ \hbar$ and excitation energy of around 13 MeV for negative parity states are presented in Tables II and III, respectively. The percentage contributions of the first two dominant configurations of the corresponding states spanning the experimentally observed range are also listed there. Comparison with experimental results for level energies are shown in Figs. 5 and 6 for positive parity and negative parity states, respectively. It is important to mention here that between the 8_1^+ and 8_2^+, 11_1^+ and 11_2^+ and 14_1^+ and 15_1^+ states, one gets several states in shell-model calculations, but we have shown only states for comparison with the experimental data. The same holds for the negative-parity states as well.

B. Low-spin states

Calculated excitation energies for the low lying states up to 7 MeV for both parities are in reasonable agreement with the experimental ones. These results can be compared with those reported earlier [15], where the difference between the observed and the calculated level energies was on the average 320 keV, in contrast to around 270 keV in the present work. The major contribution towards the structure of positive parity states comes from the configuration with proton excitations across the $Z = 40$ subshell gap, *i.e.*, $\pi[(1f_{5/2}2p)^{-2}(1g_{9/2})^2]$. For negative parity states the contributions come mainly from the $\pi[(2p)^{-1}(1g_{9/2})^1]$ and $\pi[(1f_{5/2}2p)^{-3}(1g_{9/2})^3]$ configurations.

The calculated $2_1^+ - 4_1^+ - 6_1^+ - 8_1^+$ states arise from breaking of one proton pair in the $g_{9/2}$ orbital; these states have seniority, $v = 2$. The seniority of the 8_2^+, 9_1^+ and 10_1^+ states is 4, because there is one hole in $\pi[1f_{5/2}]$,

Table II. Major components of wavefunctions for positive parity states in ^{90}Zr.

I^π	Probability	Proton	Neutron
$0^+_{\rm g.s.}$	28.15 %	$f^6_{5/2}p^4_{3/2}p^0_{1/2}g^2_{9/2}$	$g^{10}_{9/2}d^0_{5/2}$
	27.58 %	$f^6_{5/2}p^4_{3/2}p^2_{1/2}g^0_{9/2}$	$g^{10}_{9/2}d^0_{5/2}$
2^+_1	38.57 %	$f^6_{5/2}p^4_{3/2}p^0_{1/2}g^2_{9/2}$	$g^{10}_{9/2}d^0_{5/2}$
	16.53 %	$f^4_{5/2}p^4_{3/2}p^2_{1/2}g^2_{9/2}$	$g^{10}_{9/2}d^0_{5/2}$
4^+_1	42.52 %	$f^6_{5/2}p^4_{3/2}p^0_{1/2}g^2_{9/2}$	$g^{10}_{9/2}d^0_{5/2}$
	15.47 %	$f^4_{5/2}p^4_{3/2}p^2_{1/2}g^2_{9/2}$	$g^{10}_{9/2}d^0_{5/2}$
6^+_1	50.76 %	$f^6_{5/2}p^4_{3/2}p^0_{1/2}g^2_{9/2}$	$g^{10}_{9/2}d^0_{5/2}$
	13.90 %	$f^4_{5/2}p^4_{3/2}p^2_{1/2}g^2_{9/2}$	$g^{10}_{9/2}d^0_{5/2}$
8^+_1	52.36 %	$f^6_{5/2}p^4_{3/2}p^0_{1/2}g^2_{9/2}$	$g^{10}_{9/2}d^0_{5/2}$
	13.36 %	$f^4_{5/2}p^4_{3/2}p^2_{1/2}g^2_{9/2}$	$g^{10}_{9/2}d^0_{5/2}$
8^+_2	40.89 %	$f^5_{5/2}p^4_{3/2}p^1_{1/2}g^2_{9/2}$	$g^{10}_{9/2}d^0_{5/2}$
	20.68 %	$f^6_{5/2}p^3_{3/2}p^1_{1/2}g^2_{9/2}$	$g^{10}_{9/2}d^0_{5/2}$
9^+_1	68.27 %	$f^5_{5/2}p^4_{3/2}p^1_{1/2}g^2_{9/2}$	$g^{10}_{9/2}d^0_{5/2}$
	11.00 %	$f^5_{5/2}p^3_{3/2}p^2_{1/2}g^2_{9/2}$	$g^{10}_{9/2}d^0_{5/2}$
9^+_2	37.59 %	$f^6_{5/2}p^3_{3/2}p^1_{1/2}g^2_{9/2}$	$g^{10}_{9/2}d^0_{5/2}$
	24.10 %	$f^5_{5/2}p^4_{3/2}p^1_{1/2}g^2_{9/2}$	$g^{10}_{9/2}d^0_{5/2}$
10^+_1	49.87 %	$f^6_{5/2}p^3_{3/2}p^1_{1/2}g^2_{9/2}$	$g^{10}_{9/2}d^0_{5/2}$
	16.61 %	$f^5_{5/2}p^4_{3/2}p^1_{1/2}g^2_{9/2}$	$g^{10}_{9/2}d^0_{5/2}$
10^+_2	67.01 %	$f^5_{5/2}p^4_{3/2}p^1_{1/2}g^2_{9/2}$	$g^{10}_{9/2}d^0_{5/2}$
	9.68 %	$f^5_{5/2}p^3_{3/2}p^2_{1/2}g^2_{9/2}$	$g^{10}_{9/2}d^0_{5/2}$
11^+_1	67.40 %	$f^5_{5/2}p^4_{3/2}p^1_{1/2}g^2_{9/2}$	$g^{10}_{9/2}d^0_{5/2}$
	12.96 %	$f^5_{5/2}p^3_{3/2}p^2_{1/2}g^2_{9/2}$	$g^{10}_{9/2}d^0_{5/2}$
11^+_2	33.69 %	$f^6_{5/2}p^4_{3/2}p^0_{1/2}g^2_{9/2}$	$g^{9}_{9/2}d^1_{5/2}$
	18.27 %	$f^4_{5/2}p^4_{3/2}p^2_{1/2}g^2_{9/2}$	$g^{9}_{9/2}d^1_{5/2}$
12^+_1	38.39 %	$f^6_{5/2}p^4_{3/2}p^0_{1/2}g^2_{9/2}$	$g^{9}_{9/2}d^1_{5/2}$
	19.35 %	$f^4_{5/2}p^4_{3/2}p^2_{1/2}g^2_{9/2}$	$g^{9}_{9/2}d^1_{5/2}$
13^+_1	41.41 %	$f^6_{5/2}p^4_{3/2}p^0_{1/2}g^2_{9/2}$	$g^{9}_{9/2}d^1_{5/2}$
	19.26 %	$f^4_{5/2}p^4_{3/2}p^2_{1/2}g^2_{9/2}$	$g^{9}_{9/2}d^1_{5/2}$
14^+_1	40.29 %	$f^6_{5/2}p^4_{3/2}p^0_{1/2}g^2_{9/2}$	$g^{9}_{9/2}d^1_{5/2}$
	17.26 %	$f^4_{5/2}p^4_{3/2}p^2_{1/2}g^2_{9/2}$	$g^{9}_{9/2}d^1_{5/2}$
15^+_1	27.58 %	$f^6_{5/2}p^4_{3/2}p^0_{1/2}g^2_{9/2}$	$g^{9}_{9/2}d^1_{5/2}$
	25.24 %	$f^5_{5/2}p^4_{3/2}p^1_{1/2}g^2_{9/2}$	$g^{9}_{9/2}d^1_{5/2}$
15^+_2	52.18 %	$f^5_{5/2}p^4_{3/2}p^1_{1/2}g^2_{9/2}$	$g^{9}_{9/2}d^1_{5/2}$
	16.24 %	$f^6_{5/2}p^4_{3/2}p^0_{1/2}g^2_{9/2}$	$g^{9}_{9/2}d^1_{5/2}$

Table III. Major components of wavefunctions for negative parity states in ^{90}Zr.

I^π	Probability	Proton	Neutron
3^-_1	60.40 %	$f^6_{5/2}p^3_{3/2}p^2_{1/2}g^1_{9/2}$	$g^{10}_{9/2}d^0_{5/2}$
	10.86 %	$f^6_{5/2}p^3_{3/2}p^0_{1/2}g^3_{9/2}$	$g^{10}_{9/2}d^0_{5/2}$
5^-_1	74.56 %	$f^6_{5/2}p^4_{3/2}p^1_{1/2}g^1_{9/2}$	$g^{10}_{9/2}d^0_{5/2}$
	9.93 %	$f^6_{5/2}p^2_{3/2}p^1_{1/2}g^3_{9/2}$	$g^{10}_{9/2}d^0_{5/2}$
10^-_1	68.21 %	$f^5_{5/2}p^4_{3/2}p^0_{1/2}g^3_{9/2}$	$g^{10}_{9/2}d^0_{5/2}$
	10.54 %	$f^5_{5/2}p^3_{3/2}p^1_{1/2}g^3_{9/2}$	$g^{10}_{9/2}d^0_{5/2}$
10^-_2	32.79 %	$f^5_{5/2}p^4_{3/2}p^0_{1/2}g^3_{9/2}$	$g^{10}_{9/2}d^0_{5/2}$
	21.01 %	$f^4_{5/2}p^4_{3/2}p^1_{1/2}g^3_{9/2}$	$g^{10}_{9/2}d^0_{5/2}$
11^-_1	60.93 %	$f^5_{5/2}p^4_{3/2}p^0_{1/2}g^3_{9/2}$	$g^{10}_{9/2}d^0_{5/2}$
	11.81 %	$f^5_{5/2}p^3_{3/2}p^1_{1/2}g^3_{9/2}$	$g^{10}_{9/2}d^0_{5/2}$
11^-_2	33.50 %	$f^4_{5/2}p^4_{3/2}p^1_{1/2}g^3_{9/2}$	$g^{10}_{9/2}d^0_{5/2}$
	17.08 %	$f^5_{5/2}p^4_{3/2}p^0_{1/2}g^3_{9/2}$	$g^{10}_{9/2}d^0_{5/2}$
14^-_1	49.70 %	$f^5_{5/2}p^4_{3/2}p^0_{1/2}g^3_{9/2}$	$g^{9}_{9/2}d^1_{5/2}$
	10.77 %	$f^5_{5/2}p^3_{3/2}p^1_{1/2}g^3_{9/2}$	$g^{9}_{9/2}d^1_{5/2}$
15^-_1	43.82 %	$f^4_{5/2}p^4_{3/2}p^1_{1/2}g^3_{9/2}$	$g^{10}_{9/2}d^0_{5/2}$
	30.80 %	$f^5_{5/2}p^3_{3/2}p^1_{1/2}g^3_{9/2}$	$g^{10}_{9/2}d^0_{5/2}$
15^-_2	36.23 %	$f^5_{5/2}p^4_{3/2}p^0_{1/2}g^3_{9/2}$	$g^{9}_{9/2}d^1_{5/2}$
	27.48 %	$f^5_{5/2}p^4_{3/2}p^0_{1/2}g^3_{9/2}$	$g^{9}_{9/2}s^1_{1/2}$
16^-_1	52.93 %	$f^5_{5/2}p^4_{3/2}p^0_{1/2}g^3_{9/2}$	$g^{9}_{9/2}d^1_{5/2}$
	13.26 %	$f^5_{5/2}p^3_{3/2}p^1_{1/2}g^3_{9/2}$	$g^{9}_{9/2}d^1_{5/2}$
16^-_2	29.93 %	$f^5_{5/2}p^3_{3/2}p^1_{1/2}g^3_{9/2}$	$g^{9}_{9/2}d^1_{5/2}$
	27.79 %	$f^5_{5/2}p^4_{3/2}p^0_{1/2}g^3_{9/2}$	$g^{9}_{9/2}d^1_{5/2}$
16^-_3	30.57 %	$f^5_{5/2}p^4_{3/2}p^0_{1/2}g^3_{9/2}$	$g^{9}_{9/2}d^1_{5/2}$
	24.06 %	$f^4_{5/2}p^4_{3/2}p^1_{1/2}g^3_{9/2}$	$g^{9}_{9/2}d^1_{5/2}$
17^-_1	57.68 %	$f^5_{5/2}p^4_{3/2}p^0_{1/2}g^3_{9/2}$	$g^{9}_{9/2}d^1_{5/2}$
	14.92 %	$f^5_{5/2}p^3_{3/2}p^1_{1/2}g^3_{9/2}$	$g^{9}_{9/2}d^1_{5/2}$
17^-_2	33.32 %	$f^5_{5/2}p^4_{3/2}p^0_{1/2}g^3_{9/2}$	$g^{9}_{9/2}d^1_{5/2}$
	20.77 %	$f^4_{5/2}p^4_{3/2}p^1_{1/2}g^3_{9/2}$	$g^{9}_{9/2}d^1_{5/2}$
18^-_1	55.84 %	$f^5_{5/2}p^4_{3/2}p^0_{1/2}g^3_{9/2}$	$g^{9}_{9/2}d^1_{5/2}$
	16.66 %	$f^5_{5/2}p^3_{3/2}p^1_{1/2}g^3_{9/2}$	$g^{9}_{9/2}d^1_{5/2}$
18^-_2	56.12 %	$f^5_{5/2}p^3_{3/2}p^1_{1/2}g^3_{9/2}$	$g^{9}_{9/2}d^1_{5/2}$
	14.01 %	$f^4_{5/2}p^4_{3/2}p^1_{1/2}g^3_{9/2}$	$g^{9}_{9/2}d^1_{5/2}$
19^-_1	59.41 %	$f^5_{5/2}p^4_{3/2}p^0_{1/2}g^3_{9/2}$	$g^{9}_{9/2}d^1_{5/2}$
	14.57 %	$f^5_{5/2}p^3_{3/2}p^1_{1/2}g^3_{9/2}$	$g^{9}_{9/2}d^1_{5/2}$
19^-_2	57.35 %	$f^5_{5/2}p^3_{3/2}p^1_{1/2}g^3_{9/2}$	$g^{9}_{9/2}d^1_{5/2}$
	18.71 %	$f^4_{5/2}p^4_{3/2}p^1_{1/2}g^3_{9/2}$	$g^{9}_{9/2}d^1_{5/2}$
20^-_1	61.50 %	$f^5_{5/2}p^4_{3/2}p^0_{1/2}g^3_{9/2}$	$g^{9}_{9/2}d^1_{5/2}$
	11.79 %	$f^5_{5/2}p^3_{3/2}p^1_{1/2}g^3_{9/2}$	$g^{9}_{9/2}d^1_{5/2}$
20^-_2	51.04 %	$f^5_{5/2}p^3_{3/2}p^1_{1/2}g^3_{9/2}$	$g^{9}_{9/2}d^1_{5/2}$
	27.88 %	$f^4_{5/2}p^4_{3/2}p^1_{1/2}g^3_{9/2}$	$g^{9}_{9/2}d^1_{5/2}$

another hole in $\pi[2p_{1/2}]$ and they couple with the breaking of a pair in $1g_{9/2}$. The seniority of the 3^-_1 and 5^-_1 states is 2; these states result from the coupling of one proton hole in $p_{3/2}/p_{1/2}$ and one proton particle in $g_{9/2}$.

C. High-spin states

The configurations used by Warburton *et al.* to describe experimental high-spin states were $\pi[(1f_{5/2}2p)^{-n}(1g_{9/2})^n]$, where $n = 2, 4$ and $n = 1, 3$ for positive and negative parity states, respectively [15]. To generate more spin, neutron excitations were also allowed, but the calculated levels were not mentioned in Ref. [15]. Although the calculations reproduced the experimental energy levels fairly well, the calculated 12^+ level in this model space was predicted at 7784 keV, which was ~ 550 keV higher than the experimental value. On the other hand, the present calculations predict a sequence of levels – 11^+_2, 12^+_1, 13^+_1, 14^+_1, and 15^+_1 – at 7256, 7276, 7514, 8231, and 9064 keV excitation energy, respectively (see Fig. 5), having the dominant configurations $\pi[(1g_{9/2})^2]_{8^+} \otimes \nu[(1g_{9/2})^{-1}(2d_{5/2})^1]_{7^+}$ and $\pi[(1f_{5/2})^{-2}(1g_{9/2})^2]_{12^+} \otimes \nu[(1g_{9/2})^{-1}(2d_{5/2})^1]_{7^+}$ with enhanced $M1$ transitions between them. An 11^+_1 level has been predicted at 6097 keV which has

Table IV. Shell-model results for average occupancy of different orbitals for different states.

I^π	$\pi[1f_{5/2}]$	$\pi[2p_{3/2}]$	$\pi[2p_{1/2}]$	$\pi[1g_{9/2}]$	$\nu[1g_{9/2}]$	$\nu[2d_{5/2}]$	$\nu[3s_{1/2}]$
$0^+_{\rm g.s.}$	5.702	3.408	1.230	1.660	9.940	0.056	0.004
2^+_1	5.329	3.592	0.848	2.231	9.865	0.129	0.006
4^+_1	5.395	3.582	0.820	2.203	9.879	0.114	0.007
6^+_1	5.538	3.524	0.753	2.185	9.912	0.082	0.006
8^+_1	5.541	3.615	0.675	2.169	9.906	0.090	0.004
8^+_2	5.265	3.458	1.121	2.155	9.861	0.133	0.006
9^+_1	5.052	3.668	1.126	2.154	9.932	0.061	0.007
9^+_2	5.415	3.269	1.180	2.135	9.843	0.151	0.006
10^+_1	5.500	3.089	1.243	2.169	9.903	0.091	0.006
10^+_2	5.023	3.666	1.138	2.173	9.924	0.071	0.006
11^+_1	4.949	3.632	1.152	2.267	9.942	0.051	0.007
11^+_2	5.367	3.572	0.918	2.143	8.995	0.875	0.136
12^+_1	5.381	3.562	0.921	2.137	8.995	0.968	0.026
13^+_1	5.402	3.565	0.898	2.135	8.995	0.988	0.017
14^+_1	5.407	3.561	0.890	2.142	8.996	0.996	0.008
15^+_1	5.273	3.533	1.039	2.155	8.995	0.984	0.021
15^+_2	5.128	3.680	1.022	2.170	8.995	0.974	0.030
3^-_1	5.774	2.929	1.662	1.635	9.951	0.043	0.005
5^-_1	5.907	3.682	1.091	1.320	9.959	0.039	0.002
10^-_1	4.890	3.722	0.321	3.067	9.910	0.078	0.012
10^-_2	4.752	3.530	0.656	3.062	9.893	0.095	0.012
11^-_1	4.838	3.706	0.390	3.066	9.899	0.089	0.012
11^-_2	4.718	3.434	0.804	3.044	9.886	0.103	0.012
14^-_1	4.790	3.674	0.476	3.060	9.002	0.843	0.155
15^-_1	4.442	3.369	1.125	3.064	9.893	0.094	0.013
15^-_2	4.814	3.713	0.408	3.065	8.975	0.624	0.401
16^-_1	4.825	3.672	0.444	3.060	8.988	0.864	0.148
16^-_2	4.712	3.437	0.800	3.050	8.991	0.921	0.088
16^-_3	4.574	3.600	0.778	3.048	8.989	0.915	0.096
17^-_1	4.820	3.669	0.452	3.059	8.993	0.936	0.071
17^-_2	4.636	3.625	0.681	3.058	8.989	0.866	0.145
18^-_1	4.783	3.673	0.483	3.062	8.994	0.961	0.045
18^-_2	4.787	3.078	1.102	3.033	8.991	0.938	0.071
19^-_1	4.773	3.678	0.477	3.072	8.996	0.997	0.007
19^-_2	4.732	3.128	1.105	3.035	8.993	0.962	0.045
20^-_1	4.769	3.686	0.463	3.082	8.996	0.998	0.006
20^-_2	4.640	3.178	1.144	3.038	8.992	0.953	0.055

$\pi[(1f_{5/2})^{-1}(2p)^{-1}(1g_{9/2})^2]$ as most dominant configuration. One can see that the configurations of the levels of the aforementioned sequence have neutron excited structures from $1g_{9/2}$ to $2d_{5/2}$ orbital, which is completely different from the configuration of 11^+_1 level. As mentioned earlier, no γ-ray transition has been observed experimentally from 12^+_1 to 11^+_1 level due to their structural differences. The seniority of the configurations of the levels of Band-I is 4. The calculated $B(M1)$ strengths of ~ 1 W.u. of the transitions of the band are also in reasonable agreement with the experimentally observed values [15]. Noticeable feature of the structure of these states is the coupling of protons and neutrons amongst themselves in an almost stretched configuration, which then recouple to form states of different total spin. The fully aligned $\pi[(1g_{9/2})^2]_{8^+}$ structure with spin-parity of 8^+ is observed at an excitation energy of 3588 keV. The coupling of this proton structure with the neutron-core excited structure $\nu[(1g_{9/2})^{-1}(2d_{5/2})^1]_{7^+}$ forms the states of Band-I. It is to be noted that the sequence starts at an excitation energy of 3.6 MeV higher than the fully aligned proton structure. This indicates the simultaneous excitations of protons and neutrons across the $Z = 40$ and $N = 50$ shell gaps, respectively. Similar excitations have been observed in ^{88}Sr around 9 MeV idenified as 13^+ state and above for positive parity band by Stefanova *et al.* [6]. In their work, the calculated 12^+_3, 13^+_1, 14^+_1, 15^+_1, and 16^+_1 states have this configuration. Such a scenario is also observed in ^{91,92}Zr, where the states with neutron-core excited configuration lie at $\sim 4 - 4.5$ MeV higher in excitation energy than the corresponding unexcited neutron configurations

[18]. In ^{91}Zr, the $21/2^+$ state having the fully aligned $\pi[(1g_{9/2})^2]_{8^+} \otimes \nu[(2d_{5/2})^1]_{5/2^+}$ configuration is observed at 3166 keV excitation energy. This configuration couples to the aforementioned neutron-core excited configuration to form a sequence at ~ 7 MeV excitation energy starting with the $27/2^+$ state. In ^{92}Zr, the states above the $I^\pi = (17^+)$ lying at ~ 9.6 MeV excitation energy correspond to the coupling of the neutron core excitation structure and the fully-aligned (12^+) state at 4948 keV.

For negative parity states with spin higher than $I = 15$ $\hbar$, an additional excitation of proton across the $Z = 40$ subshell to the $g_{9/2}$ orbital is required. Therefore, the following configurations are suggested to form the dominant part of the structure of the states of negative-parity Band-II and Band-III : $\pi[(1f_{5/2})^{-1}(2p_{1/2})^{-2}(1g_{9/2})^3] \otimes \nu[(1g_{9/2})^{-1}(2d_{5/2})^1]$, $\pi[(1f_{5/2})^{-2}(2p_{1/2})^{-1}(1g_{9/2})^3] \otimes \nu[(1g_{9/2})^{-1}(2d_{5/2})^1]$, and $\pi[(1f_{5/2})^{-1}(2p_{3/2})^{-1}(2p_{1/2})^{-1}(1g_{9/2})^3] \otimes \nu[(1g_{9/2})^{-1}(2d_{5/2})^1]$. These configurations have seniority ranging from $v = 4$ to 6. Similar to Band-I, the high-spin states in these bands are generated by the recoupling of nearly stretched proton and neutron configurations.

The configuration with neutron particle-hole excitation across the $N = 50$ shell gap has been observed to be a major component of the structure of high-spin yrast states of nuclei in this mass region [6, 8, 16, 17, 33]. This is because of the role of an additional neutron hole in the $g_{9/2}$ orbital in contributing to the spin of these yrast states. These high-spin states form a band-like structure with enhanced $M1$ transitions, similar to what has been observed in ^{90}Zr. As mentioned above, these configurations have stretched proton and neutron configurations, and high-spin is generated by their recoupling.

In Table IV, we have shown the average occupancy of different orbitals corresponding to different states. The occupancy of $\nu[3s_{1/2}]$ and $\nu[2d_{5/2}]$ orbitals are increasing with spin. It reflects the importance of the inclusion of neutron orbitals beyond the $N = 50$ shell for high-spin states.

V. SUMMARY

The level scheme of ^{90}Zr has been substantially extended with the addition of thirty-two new transitions. The spin-parity of different states up to spin 20 $\hbar$ and excitation energy ~ 13 MeV have been established on the basis of angular distribution, angular correlation and polarization measurements. One of the important features of the present level scheme is the presence of two $\Delta I = 1$, $M1$ sequences at higher spins. The shell-model calculations, with the extended model space including neutron excitations across the $N = 50$ shell gap, give a good description of both the positive as well as the negative parity states up to highest observed excitation energy and spins. This indicates the dominance of single-particle excitations in this nucleus. The role of occupancy of neutrons in $2d_{5/2}$ and $3s_{1/2}$ beyond $N = 50$ shell gap for the description of high-spin states has been highlighted.

VI. ACKNOWLEDGEMENTS

Authors are grateful to the staff at TIFR-BARC Pelletron Linac Facility for providing good quality beam and smooth operation of the accelerator for the entire duration of the experiment. The help and cooperation from B. Naidu, S. Jadhav, Abraham T. Vazhappilly and R. Donthi in the setting up of the experiment is acknowledged. This work is supported by the Department of Atomic Energy, Government of India (Project Identification Code: 12-R&D-TFR-5.02-0200) and the Department of Science and Technology, Government of India (Grant No. IR/S2/PF-03/2003-II). R.P. and E.I. acknowledge the RCNP Collaboration Research network (COREnet) program. E.I. acknowledges the support by the International Joint Research Promotion Program of Osaka University and JSPS KAKENHI Grant Number JP17H02893. U.G. acknowledges the U. S. National Science Foundation (Grant No. PHY-2011890). D.N. would like to acknowledge the financial support from the CSIR, India towards this project. P.C.S. acknowledges a research grant from SERB (India), CRG/2019/000556.

[1] H. C. Chiang, M. C. Wang, and C. S. Han, J. Phys. G **6**, 345 (1980).
[2] G. Winter, R. Schwengner, J. Reif, H. Prade, L. Funke, R. Wirowski, N. Nicolay, A. Dewald, P. von Brentano, H. Grawe, and R. Schubart, Phys. Rev. C **48**, 1010 (1993).
[3] A. Astier, M.-G. Porquet, Ts. Venkova, G. Duchêne, F. Azaiez, D. Curien, I. Deloncle, O. Dorvaux, B. J. P. Gall, N. Redon, M. Rousseau, and O. Stézowski, Phys. Rev. C **88**, 024321 (2013).
[4] L. Käubler, K. D. Schilling, R. Schwengner, F. Dönau, E. Grosse, D. Belic, P. von Brentano, M. Bubner, C. Fransen, M. Grinberg, U. Kneissl, C. Kohstall, A. Linnemann, P. Matschinsky, A. Nord, N. Pietralla, H. H. Pitz, M. Scheck, F. Stedile, and V. Werner, Phys. Rev. C **65**, 054315 (2002).

[5] J. J. Liu, Y. Zheng, H. B. Sun, X. G. Wu, C. Y. He, G. S. Li, C. B. Li, S. H. Yao, H. W. Li, S. P. Hu, J. L. Wang, W. W. Qu, C. Xu, and J. J. Sun, Eur. Phys. J. A **50**, 84 (2014).

[6] E. A. Stefanova, R. Schwengner, J. Reif, H. Schnare, F. Dönau, M. Wilhelm, A. Fitzler, S. Kasemann, P. von Brentano, and W. Andrejtscheff, Phys. Rev. C **62**, 054314 (2000).

[7] E. A. Stefanova, R. Schwengner, G. Rainovski, K. D. Schilling, A. Wagner, F. Dönau, E. Galindo, A. Jungclaus, K. P. Lieb, O. Thelen, J. Eberth, D. R. Napoli, C. A. Ur, G. de Angelis, M. Axiotis, A. Gadea, N. Marginean, T. Martinez, Th. Kröll, and T. Kutsarova, Phys. Rev. C **63**, 064315 (2001).

[8] R. Schwengner, J. Reif, H. Schnare, G. Winter, T. Servene, L. Käubler, H. Prade, M. Wilhelm, A. Fitzler, S. Kasemann, E. Radermacher, and P. von Brentano, Phys. Rev. C **57**, 2892 (1998).

[9] C. J. Xu, S. Y. Wang, C. Y. Niu, C. Liu, B. Qi, D. P. Sun, L. Liu, P. Zhang, Z. Q. Li, Z. Wang, X. G. Wu, G. S. Li, C. Y. He, Y. Zheng, B. B. Yu, C. B. Li, S. P. Hu, S. H. Yao, Y. H. Wu, X. P. Cao, and J. L. Wang, Phys. Rev. C **86**, 027302 (2012).

[10] M. Bunce, P. H. Regan, V. Werner, C. W. Beausang, V. Anagnostatou, M. Bowry, R. J. Casperson, D. Chen, N. Cooper, P. M. Goddard, R. O. Hughes, G. Ilie, P. J. R. Mason, B. Pauerstein, M. W. Reed, T. J. Ross, and E. C. Simpson, Phys. Rev. C **87**, 044337 (2013).

[11] L. Funke, G. Winter, J. Döring, L. Käubler, H. Prade, R. Schwengner, E. Will, Ch. Protochristov, W. Andrejtschef, L. G. Kostova, P. O. Lipas, and R. Wirowski, Nucl. Phys. A **541**, 241 (1992).

[12] J. Reif, G. Winter, L. Käubler, H. Prade, and R. Schwengner, Nucl. Phys. A **587**, 449 (1995).

[13] G. Rainovski, R. Schwengner, K. D. Schilling, A. Wagner, A. Jungclaus, E. Galindo, O. Thelen, D. R. Napoli, C. A. Ur, G. de Angelis, M. Axiotis, A. Gadea, N. Marginean, T. Martinez, and Th. Kröll, Phys. Rev. C **65**, 044327 (2002).

[14] D. Bucurescu, Zs. Podolyák, C. Rusu, G. de Angelis, Y. H. Zhang, G. Căta-Danil, I. Căta-Danil, M. Ivaşcu, N. Mărginean, R. Mărginean, L. C. Mihăilescu, G. A. Suliman, P. H. Regan, W. Gelletly, S. D. Langdown, J. J. Valiente Dobón, D. Bazzacco, S. Lunardi, C. A. Ur, M. Axiotis, A. Gadea, E. Farnea, M. Ionescu-Bujor, A. Iordăchescu, Th. Kröll, T. Martinez, P. G. Bizzetti, R. Broda, N. H. Medina, B. Quintana, and B. Rubio, Phys. Rev. C **71**, 034315 (2005).

[15] E. K. Warburton, J. W. Olness, C. J. Lister, R. W. Zurmühle, and J. A. Becker, Phys. Rev. C **31**, 1184 (1985).

[16] S. Saha, R. Palit, J. Sethi, S. Biswas, P. Singh, T. Trivedi, D. Choudhury, and P. C. Srivastava, Phys. Rev. C **89**, 044315 (2014).

[17] S. Saha, R. Palit, J. Sethi, T. Trivedi, P. C. Srivastava, S. Kumar, B. S. Naidu, R. Donthi, S. Jadhav, D. C. Biswas, U. Garg, A. Goswami, H. C. Jain, P. K. Joshi, G. Mukherjee, Z. Naik, S. Nag, V. Nanal, R. G. Pillay, S. Saha, and A. K. Singh, Phys. Rev. C **86**, 034315 (2012).

[18] Z. G. Wang, M. L. Liu, Y. H. Zhang, X. H. Zhou, S. Guo, J. G. Wang, X. G. Lei, Y. Zheng, Y. D. Fang, Y. H. Qiang, N. T. Zhang, B. Ding, G. S. Li, F. Ma, X. L. Yan, S. C. Wang, B. S. Gao, F. Fang, B. T. Hu, X. G. Wu, C. Y. He, and Y. Zheng, Phys. Rev. C **89**, 044308 (2014).

[19] Purnima Singh, R. Palit, S. Saha, J. Sethi, S. Biswas, D. Choudhury, P. C. Srivastava, and T. Trivedi, Phys. Rev. C **90**, 014306 (2014).

[20] X. Z. Cui, L. Z. Zhu, X. G. Wu, Z. M. Wang, C. Y. He, Y. Liu, G. S. Li, S. X. Wen, P. Zhang, R. Meng, R. G. Ma, P. Luo, Y. Zheng, M. M. Ndontchueng, J. D. Huo, and C. X. Yang, Phys. Rev. C **72**, 044322 (2005).

[21] P. W. Luo, X. G. Wu, H. B. Sun, G. S. Li, C. Y. He, Y. Zheng, C. B. Li, S. P. Hu, Y. H. Wu, H. W. Li, J. J. Liu, J. L. Wang, S. H. Yao, and Scott A. Edwards, Phys. Rev. C **89**, 034318 (2014).

[22] S. Ray, N. S. Pattabiraman, R. Goswami, S. S. Ghugre, A. K. Sinha, and U. Garg, Phys. Rev. C **69**, 054314 (2004).

[23] N. S. Pattabiraman, S. N. Chintalapudi, S. S. Ghugre, B. V. Tirumala Rao, M. L. N. Raju, T. Seshi Reddy, P. K. Joshi, R. Palit, and H. C. Jain, Phys. Rev. C **65**, 044324 (2002).

[24] T. Fukuchi, Y. Gono, A. Odahara, S. Tanaka, M. Inoue, Y. Wakabayashi, T. Sasaki, M. Kibe, N. Hokoiwa, T. Shinozuka, M. Fujita, A. Yamazaki, T. Sonoda, C. S. Lee, Y. K. Kwon, J. Y. Moon, and J. H. Lee, Eur. Phys. J. A **24**, 249 (2005).

[25] B. Kharraja, S. S. Ghugre, U. Garg, R. V. F. Janssens, M. P. Carpenter, B. Crowell, T. L. Khoo, T. Lauritsen, D. Nisius, W. Reviol, W. F. Mueller, L. L. Riedinger, and R. Kaczarowski, Phys. Rev. C **57**, 2903 (1998).

[26] D. Rudolph, C. J. Gross, A. Harder, M. K. Kabadiyski, K. P. Lieb, M. Weiszflog, J. Altmann, A. Dewald, J. Eberth, T. Mylaeus, H. Grawe, J. Heese, and K.-H. Maier, Phys. Rev. C **49**, 66 (1994).

[27] M. Hausmann, A. Jungclaus, E. Galindo, K. P. Lieb, O. Yordanov, I. P. Johnstone, R. Schwengner, A. Dewald, A. Fitzler, O. Möller, G. de Angelis, A. Gadea, T. Martinez, D. R. Napoli, and C. Ur, Phys. Rev. C **68**, 024309 (2003).

[28] S. S. Ghugre, B. Kharraja, U. Garg, R. V. F. Janssens, M. P. Carpenter, B. Crowell, T. L. Khoo, T. Lauritsen, D. Nisius, W. Reviol, W. F. Mueller, L. L. Riedinger, and R. Kaczarowski, Phys. Rev. C **61**, 024302 (1999).

[29] F. Ghazi Moradi, C. Qi, B. Cederwall, A. Ataç, T. Bäck, R. Liotta, M. Doncel, A. Johnson, G. de France, E. Clément, A. Dijon, R. Wadsworth, T. W. Henry, A. J. Nichols, H. Al-Azri, J. Nyberg, A. Gengelbach, T. Hüyük, B. M. Nyakó, J. Timár, D. Sohler, Zs. Dombrádi, I. Kuti, K. Juhász, M. Palacz, G. Jaworski, S. M. Lenzi, P. R. John, D. R. Napoli, A. Gottardo, V. Modamio, A. Di Nitto, B. Yilmaz, Ö. Aktas, and E. Ideguchi, Phys. Rev. C **89**, 014301 (2014).

[30] E. Galindo, M. Hausmann, A. Jungclaus, K. P. Lieb, O. Yordanov, I. P. Johnstone, R. Schwengner, A. Dewald, A. Fitzler, O. Möller, G. de Angelis, A. Gadea, T. Martinez, D. R. Napoli, and C. Ur, Phys. Rev. C **69**, 024304 (2004).

[31] A. Jungclaus, D. Kast, K. P. Lieb, C. Teich, M. Weiszflog, T. Härtlein, C. Ender, F. Köck, D. Schwalm, J. Reif, R. Peusquens, A. Dewald, J. Eberth, H.-G. Thomas, M. Górska, and H. Grawe, Nucl. Phys. A **637**, 346 (1998).

[32] R. Schwengner, G. Winter, J. Reif, H. Prade, L. Käubler, R. Wirowski, N. Nicolay, S. Albers, S. Eβer, P. von Brentano, and W. Andrejtscheff, Nucl. Phys. A **584**, 159 (1995).

[33] P. Banerjee, S. Ganguly, M. K. Pradhan, Md. Moin Shaikh, H. P. Sharma, S. Chakraborty, R. Palit, R. G. Pillay, V. Nanal, S. Saha, and J. Sethi, Phys. Rev. C **98**,

034320 (2018).
[34] S. Saha, R. Palit, J. Sethi, S. Biswas, P. Singh, S. Nag, A. K. Singh, I. Ragnarsson, F. S. Babra, U. Garg, A. Goswami, E. Ideguchi, H. C. Jain, S. Kumar, Md. S. R. Laskar, G. Mukherjee, Z. Naik, and C. S. Palshetkar, Phys. Rev. C **99**, 054301 (2019).
[35] H. Wang, K. Ma, S. Liu, and J. Lu, Chin. Phys. C **45**, 094106 (2021).
[36] R. Palit, in *Application of Accelerators in Research and Industry: Twenty-First International Conference*, edited by F. D. McDaniel and B. L. Doyle, AIP Conf. Proc. No. 1336 (AIP, New York, 2011), p. 573.
[37] H. Tan *et al.*, in *Nuclear Science Symposium Conference Record 2008* (IEEE, Washington, DC, 2008), p. 3196.
[38] R. Palit, S. Saha, J. Sethi, T. Trivedi, S. Sharma, B. S. Naidu, S. Jadhav, R. Donthi, P. B. Chavan, H. Tan, and W. Hennig, Nucl. Instrum. Methods Phys. Res. A **680**, 90 (2012).
[39] D. C. Radford, Nucl. Instrum. Methods Phys. Res. A **361**, 297 (1995).
[40] D. C. Radford, Nucl. Instrum. Methods Phys. Res. A **361**, 306 (1995).
[41] P. J. Twin, in *The Electromagnetic Interaction in Nuclear Spectroscopy*, edited by W. D. Hamilton (North-Holland, Amsterdam, 1975), p. 701.
[42] A. Krämer-flecken, T. Morek, R. M. Lieder, W. Gast, G. Hebbinghaus, H. M. Jäger, and W. Urban, Nucl. Instrum. Methods Phys. Res. A **275**, 333 (1989).
[43] K. S. Krane, R. M. Steffen, and R. M. Wheeler, At. Data Nucl. Data Tables **11**, 351 (1973).
[44] P. M. Jones, L. Wei, F. A. Beck, P. A. Butler, T. Byrski, G. Duchne, G. de France, F. Hannachi, G. D. Jones, and B. Kharraja, Nucl. Instrum. Methods Phys. Res. A **362**, 556 (1995).
[45] Ch. Droste, S. G. Rohozińsky, K. Starosta, T. Morek, J. Srebrny, and P. Magierski, Nucl. Instrum. Methods Phys. Res. A **378**, 518 (1996).
[46] GTOL code, see `https://www-nds.iaea.org/public/ensdf_pgm/`.
[47] S. K. Basu, and E. A. McCutchan, Nuclear Data Sheets **165**, 1 (2020).
[48] J. A. Becker, S. D. Bloom, and E. K. Warburton, Amer. Chem. Soc. Symposium Series **324**, 78 (1986).
[49] N. Shimizu, T. Mizusaki, Y. Utsuno, and Y. Tsunoda, Comput. Phys. Commun. **244**, 372 (2019).
[50] A. Hosaka, K.-I. Kubo, and H. Toki, Nucl. Phys. A **444**, 76 (1985).
[51] Xiangdong Ji, and B. H. Wildenthal, Phys. Rev. C **37**, 1256 (1988).
[52] D. H. Gloeckner, Nucl. Phys. A **253**, 301 (1975).
[53] F. J. D. Serduke, R. D. Lawson, and D. H. Gloeckner, Nucl. Phys. A **256**, 45 (1976).
[54] D. Bucurescu, C. Rusu, N. Mărginean, C. A. Ur, G. de Angelis, L. Corradi, D. Bazzacco, S. Beghini, F. Della Vedova, G. Duchene, E. Farnea, T. Faul, E. Fioretto, A. Gadea, W. Gelletly, B. Guiot, M. Ionescu-Bujor, A. Iordăchescu, S. D. Langdown, S. M. Lenzi, S. Lunardi, P. Mason, C. Mihai, R. Mărginean, R. Menegazzo, G. Montagnoli, D. Napoli, Zs. Podolyák, P. H. Regan, F. Scarlassara, A. M. Stefanini, G. A. Suliman, S. Szilner, M. Trotta, J. J. Valiente Dobón, and Y. H. Zhang, Phys. Rev. C **76**, 064301 (2007).